Experimental investigation on the influence of wind direction on the aerodynamic loads acting on low aspect-ratio triangular prisms

Giacomo Valerio Iungo and Guido Buresti
Department of Aerospace Engineering, University of Pisa, Italy
E-mail: giacomo.iungo@unipi.it, g.buresti@unipi.it

Keywords: Bluff-body aerodynamics, triangular prisms, wakes, vorticity dynamics.

SUMMARY. The results are described of wind-tunnel measurements of the mean and fluctuating forces acting on low aspect-ratio triangular prisms placed vertically on a plane, having isosceles triangular cross-section with 60° or 90° apex angles and aspect ratios ranging from 1.0 to 3.0. The tests are carried out by varying the wind direction, θ, between 0° and 180°, at a Reynolds number Re $\cong 1.2 \cdot 10^5$. Furthermore, for the model with apex angle of 60° and aspect ratio 3.0, flow visualizations with tufts and hot-wire measurements are performed, which permit to characterize the wake morphology as a function of wind direction and to assess that an alternate vortex shedding always exists, with a frequency that is roughly inversely proportional to the wake width. The force measurements show that large variations in the mean values of the drag and cross-flow forces occur by varying θ, in strict connection with changes in wake flow features. The intensity of the fluctuating cross-flow forces, directly connected with vortex shedding, is found to vary significantly with flow orientation and aspect ratio, and to be approximately proportional to the streamwise projection of the body surface immersed in the separated wake. Finally, an increase in vortex shedding frequency is generally found with decreasing aspect ratio.

1 INTRODUCTION

The aerodynamic forces acting on finite-length cylindrical or prismatic bluff bodies placed vertically on a plane and immersed in a cross-flow are strictly dependent on the characteristics of the wakes they produce. In particular, the presence of velocity fluctuations induces fluctuating pressure forces on the bodies, which are a function, in general, of the body cross-section shape, of the body aspect ratio and of the incoming wind direction.

The main feature characterizing the aerodynamics of finite-length cylinders is the flow passing over the free-end, which strongly affects the wake flow field; in particular, increasingly significant three-dimensionality is introduced with decreasing body aspect-ratio, which influences the alternate vortex shedding from the sides of the body, in terms of both frequency and regularity.

Considering the flow around a finite circular cylinder, which is the bluff body to which most investigations were devoted, for values of the aspect ratio $h/d > 10$ (where h is the height and d is the diameter of the cylinder) a clear alternate vortex shedding from most of the cylinder span is observed, with Strouhal numbers of the same order as those typical of two-dimensional flow ([1] and [2]). However, a decrease of the frequency was found in a zone approaching the free-end of the cylinders, probably due to a widening of the wake caused by the flow passing over the free-end and to an increase in the formation length of the shed vortices.

Further results, including also the effect of the incoming boundary layer thickness, are available for circular cylinders of different aspect ratio (see, e.g., [3], [4], [5]). One of the most interesting features arising from these investigations is the presence of a couple of counter-rotating vortices detaching from the free-end, which produce a significant downflow in the inner region of the near wake and an increasing influence on the wake development as the aspect ratio is decreased.

As for the present work, the choice of testing prisms with triangular cross-section was mainly dictated by the small Reynolds number dependence of this geometry (due to the presence of sharp edges fixing the boundary layer separation), and by the possibility of obtaining quite different geometrical and flow conditions by varying the orientation of the models to the wind. Furthermore, very limited data are available in the literature for this body shape and for models placed with different wind directions (see, e.g., [6], [7], [8], [9]).

In [10] and [11] the wake flow fields of triangular prisms placed vertically on a plane and having two different isosceles cross-sections (with apex angles of $60°$ and $90°$) were analysed through hot-wire measurements; the aspect ratio, h/w (where w is the width of the base side of the triangular cross-sections), was varied between 1.0 and 3.0. Two wind directions, θ, were considered, and the alternate vortex shedding from the lateral vertical edges of the prisms with equilateral triangular cross-section was found to be characterized by a Strouhal number St $= fw/U_\infty \cong 0.1$ when the incoming flow impinged orthogonally to a vertical face of the models ($\theta = 0°$), whereas a dominant frequency corresponding to St $\cong 0.16$ was detected when the wind was directed against the apex edge of the prisms ($\theta = 180°$).

The higher complexity of the upper near-wake flow field when a prism with triangular cross-section and aspect ratio $h/w = 3$ was orientated with its apex edge against the incoming wind was deeply characterized in [12]. Flow fluctuations at three prevailing frequencies were singled out, with different relative intensities depending on the wake regions. In particular, the frequency connected with alternate vortex shedding from the vertical edges of the prism was found to dominate in the regions just outside the lateral boundary of the wake. On the other hand, a lower frequency, at St $\cong 0.05$, was found to prevail in the velocity fluctuations on the whole upper wake. Fluctuations with a dominating frequency significantly below that of vortex shedding had already been detected in the upper portions of the wake of finite circular cylinders with higher aspect ratio, e.g. by [3] and by [4]. Simultaneous measurements carried out over the wake of the prisms at symmetrical locations with respect to the symmetry plane showed that these fluctuations correspond to a vertical, in-phase, oscillation of two counter-rotating axial vortices detaching from the front edges of the free-end. This finding was confirmed by the results of a LES simulation of the same flow configuration, described in [13]. In [12] wake velocity fluctuations were also observed at an intermediate frequency St $\cong 0.09$, and were found to prevail in the symmetry plane. By using the evidence provided by the abovementioned LES simulation, by flow visualizations and by pressure measurements over the prism surface (see also [14]), it was suggested that these fluctuations may be caused by a flag-like oscillation of the sheet of transversal vorticity shed from the rear edge of the body free-end, and approximately lying along the downstream boundary of the recirculation region in the central part of the near wake.

The aim of the present work is to better understand the influence of the variation of the wind direction on the wake flow features and on the mean and fluctuating forces acting on triangular prisms with two different cross-sections and aspect ratio between 1.0 and 3.0. The experimental set-up is described in Section 2. In Section 3 the results of force measurements performed by varying the wind direction from $\theta = 0°$ up to $\theta = 180°$ are reported and described. Finally, conclusions are provided in Section 4.

2 EXPERIMENTAL SET-UP AND PROCEDURES

The tests were carried out in a closed-return subsonic wind tunnel, with circular open test section 1.1 m in diameter and 1.48 m in length, and free-stream turbulence level of 0.9%. The general set-up of the tests is shown in Fig. 1.

Prismatic bodies with two different isosceles triangular cross-sections were used, with apex angles of 60° (i.e. with equilateral section, denoted as model 60) or 90° (model 90), and with aspect ratios $h/w = 1.0$, 1.5, 2.0 and 3.0 (where $w = 90$ mm). The models were placed vertically on a horizontal plane, and were connected to a six-component strain-gage balance supported by a rotatable base placed underneath, so that they could easily be orientated in different wind directions, with the rotation occurring around an axis passing through the centre of gravity of their base section. The used frame of reference is shown in Fig. 1; the x-axis was chosen in the free-stream direction and the z-axis in the vertical direction, positive from the model base to the tip. The y direction was consequently defined, producing a right-hand reference frame. The analysed flow directions were generally varied in 10° intervals from $\theta = 0^\circ$, i.e. with the free-stream directed orthogonally to the larger vertical face, to $\theta = 180^\circ$, i.e. with the incoming flow directed against the apex edge of the prism. Preliminary force measurements for model 60 with $h/w = 3.0$ were carried out by varying the velocity in the range $15 \div 25$ m/s, in order to check the constancy of the Strouhal number of the spectral peak connected with vortex shedding. Subsequently, all models were tested at a free-stream velocity $U_\infty = 20$ m/s, corresponding to a Reynolds number $\mathrm{Re} = U_\infty w/\nu \cong 1.2 \cdot 10^5$. The thickness of the turbulent boundary layer on the plane, δ, was of the order of 15 mm, so that the parameter h/δ ranged from 6 to 18.

As for the force measurements, the six signals from the balance, each comprising 65536 samples, were simultaneously acquired at a sampling rate of 1 kHz, and were processed by means of the balance calibration matrix to obtain the time histories of the load components acting on the models. The maximum error of the balance measurements was previously estimated to be about 1.5%.

3 FORCE MEASUREMENTS

3.1 Mean forces

The variations with wind direction, θ, and aspect ratio, h/w, of the mean drag and cross-flow force coefficients, C_D and C_L, are shown in Fig. 2 for model 60, while the analogous data for model 90 are given in Fig. 3. The reference surface for the coefficients in these figures is hw. As can be seen, the absolute values of the force coefficients tend to slightly decrease with decreasing aspect ratio due to the three-dimensionality of the flow generated by the body free-end; however, this trend is not a remarkable one.

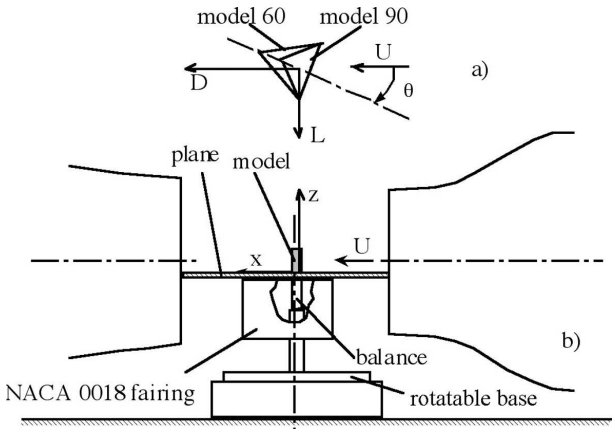

Figure 1: Experimental layout.

Considering the two extreme flow orientations, for $\theta = 0^\circ$ the two model types are characterized by a different streamwise extension of the afterbody (i.e. of the portion of body surface immersed in the separated wake), while they are identical as regards the forebody (which is a rectangular flat surface orthogonal to the free-stream). Conversely, for $\theta = 180^\circ$ (or $\theta = 60^\circ$ for model 60) the forebodies are different and the afterbody is the same. For these two orientations the corresponding drag coefficients for the two-dimensional case are available from [15], and are reported for comparison in Figs. 2(a) and 3(a). On the other hand, the available data on the variation of the forces

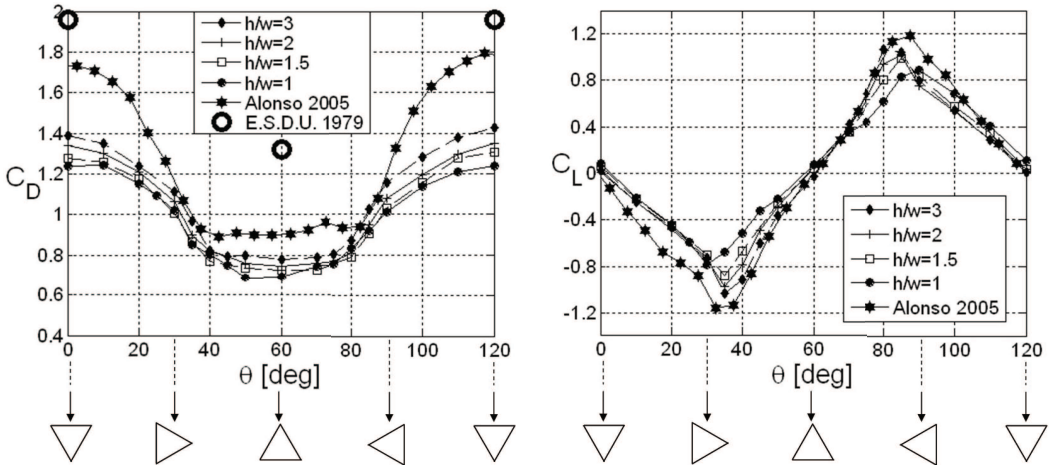

a) b)

Figure 2: Mean forces acting on model 60 with different aspect ratios, as a function of wind direction, θ: a) mean drag coefficient, C_D; b) mean cross-flow force coefficient, C_L.

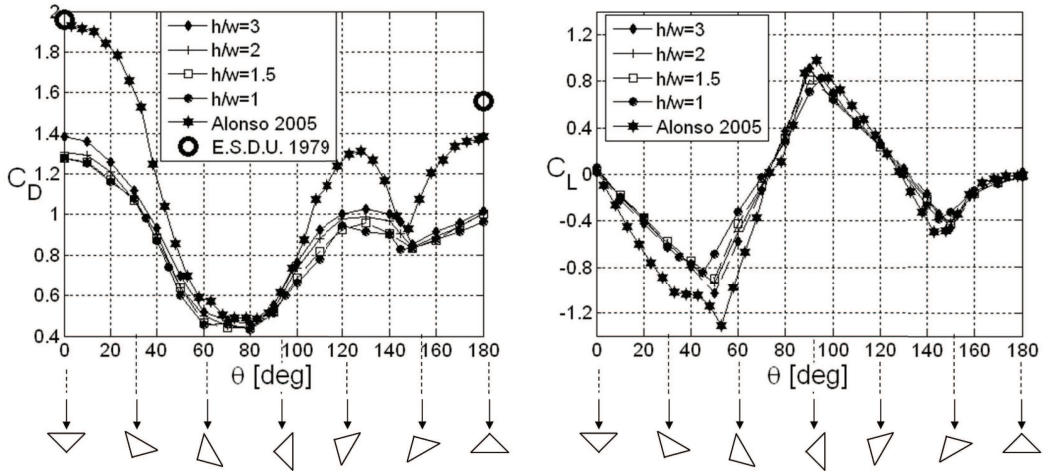

a) b)

Figure 3: Mean forces acting on model 90 with different aspect ratios, as a function of wind direction, θ: a) mean drag coefficient, C_D; b) mean cross-flow force coefficient, C_L.

with wind direction for the models considered in the present investigation are very limited even for the two-dimensional case. Actually, to the authors' knowledge the only experimental investigation regarding the effect of wind orientation for cylinders with isosceles triangular cross-sections with various apex angles is described in [9], and the relevant data are also shown in Figs. 2 and 3.

A point that is apparent from these figures is that, for the wind directions for which the comparison is possible, the two-dimensional values reported in [9] are generally lower than those given in [15]. Particularly puzzling are the results for $\theta = 0^\circ$, for which equal values are given for both models in [15] and also similar ones are found in the present investigation, whereas considerably different values are reported in [9]. It must also be pointed out that in the tests described in the latter work the forces on a triangular cylinder with apex angle of 30° were also measured as a function of θ; however, even for that case the reported values are significantly lower, for all wind directions, than those obtained in [6] for a similar cylinder. The origin of these discrepancies is not clear, although experimental uncertainties, connected, for instance, with the reference velocity or with the value of the blockage ratio (which in [9] was up to 12.5%, and varied with wind orientation) might have an influence on the obtained data.

As regards a detailed analysis of the present results, it is seen that for $\theta = 0^\circ$ both model 60 and model 90 are characterized by almost the same drag coefficient, but a certain decrease is found with decreasing aspect ratio. Conversely, when the models are placed with their apex edge against the incoming flow, a lower drag is found for model 60, as expected. An interesting point is that the ratios between the present values and the two-dimensional ones given in [15] show non-negligible differences for the various models and wind orientations. For instance, for $h/w = 3.0$ the ratios are approximately 0.71, 0.65 and 0.6, respectively for both models at $\theta = 0^\circ$, for model 90 at $\theta = 180^\circ$ and for model 60 at $\theta = 180^\circ$ (or $\theta = 60^\circ$). These differences might be explained with the different behaviour of the flow rounding the free-end of the models in the various configurations.

Let us now consider in more detail the trends obtained for model 60 (Fig. 2). Starting from $\theta = 0^\circ$, i.e. with a vertical face set normal to the wind direction, the flow is separated on the two lateral faces, so that a monotone reduction of the mean drag coefficient is found with increasing θ, consistently with the reduction of the wake cross-flow width. The latter was evaluated through hot-wire measurements, not reported here for the sake of brevity (see [16] for more details), from the transversal distance between the two typical peaks of the standard deviation detected from a traverse carried out in the cross-flow direction. The wake width, w_w, is compared in Fig. 4 with the model geometrical cross-flow width, w^*.

Subsequently, between $\theta = 35^\circ$ and $\theta = 40^\circ$ a reattachment of the flow on the leeward surface has been detected from the flow visualizations and the hot-wire measurements reported in [16], and a negative peak of the cross-flow force is observed in Fig. 2(b). By further increasing θ ($40^\circ \leq \theta \leq 60^\circ$), the wake detaches from the two rear vertical edges and a widening of the wake has been observed from the hot-wire measurements, whereas a limited further reduction of C_D is found. This different behaviour may be ascribed to the significant change of the structure of the wake flow occurring when model 60 is oriented with $40^\circ \leq \theta \leq 60^\circ$. As a matter of fact, the presence of the couple of counter-rotating vortices detaching from the front edges of the free-end produces a significant downwash flow, which interacts with the wake. Furthermore, the downwash caused by the axial vortices is probably strictly linked to the strong recirculating flow which was found to be present in the near wake for the same case; as shown in [14], this flow gives rise to an increase in the pressure acting over the lower part of the rear face of the prism, which might explain a lower drag coefficient than would be expected from the variation of the width of the wake.

For wind directions $60^\circ \leq \theta \leq 120^\circ$ the trend of C_D is symmetric due to the equilateral cross-

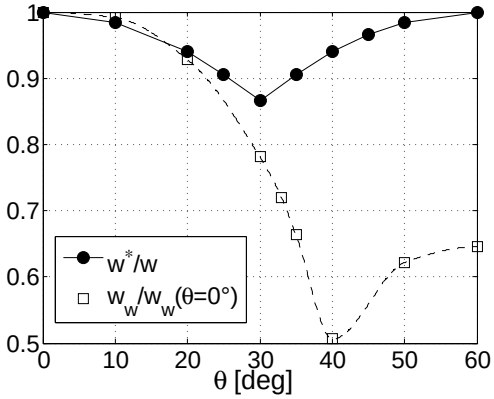

Figure 4: Comparison of the model cross-flow width, w^*, wake cross-flow width, w_w, evaluated from the hot-wire measurements for different wind directions, θ.

section of model 60, so that C_D increases with a monotone trend, while the cross-flow force coefficient, C_L, is antisymmetric and reaches its maximum value around $\theta \cong 85°$, i.e. when the flow becomes again completely separated from the leeward surface.

As for the variation of the cross-flow force coefficient, C_L, reported in Fig. 2(b), it can also be observed that the peak values, corresponding to the flow separation from the leeward surface, occur for slightly different wind directions by varying the model aspect ratio, h/w. In effect, starting from $\theta = 60°$ and increasing θ, the maximum value of C_L occurs at approximately $\theta = 85°$ for the model with $h/w = 3.0$, whereas for $h/w = 1.0$ it occurs, with a smaller absolute value, at $\theta = 90°$. Analogously, when θ is decreased the negative peak is found at $\theta = 35°$ for $h/w = 3.0$ and at $\theta = 30°$ for $h/w = 1.0$. Therefore the slope of the lift coefficient, C_L, decreases with reducing aspect ratio. This behaviour can be ascribed to the flow reattachment occurring in proximity to the model tip due to the up-wash generated by the tip vortices; as expected, this effect becomes more and more important as the model aspect ratio is decreased.

For model 90 no flow visualizations or velocity measurements were carried out in the present investigation, so that a characterization of the wake morphology can be performed only through a synergic analysis, for the different wind directions, of the force coefficients, reported in Figs. 3(a) and 3(b), and of the model cross-flow width, w^*/w. Moreover, the wake features can also be inferred from an analysis of the detailed pressure measurements described in [7] for a two-dimensional triangular cylinder with a $90°$ apex angle.

Starting from the wind direction $\theta = 0°$, i.e. with the largest vertical face set normal to the wind direction, the flow stagnation point is located on this face in correspondence to the symmetry plane and the flow is separated over the two lateral faces. With increasing θ, from the pressure measurements reported in [7] the stagnation point is seen to move towards the front vertical edge; consistently, a monotone reduction of C_D is found in the present results, following the decrease of the model cross-flow width, while the modulus of C_L increases due to the loss of flow symmetry.

From the abovementioned pressure measurements, it can be deduced that in the $2D$ case a flow reattachment on the leeward face occurs at $\theta = 55°$, which is consistent with the peak of C_L observed around $\theta = 50°$ from the present experimental campaign (the force values for $\theta = 55°$ are not available because an angular step of $10°$ was used) and with the analogous one also found at

$\theta = 55^\circ$ in [9]. For the model with aspect ratio $h/w = 1.0$ the peak of the cross-flow force coefficient is observed at $\theta = 45^\circ$, indicating that the flow reattachment on the leeward surface occurs for smaller values of θ with decreasing aspect ratio; as already mentioned for model 60, this feature may be due to the increased influence of the upwash generated from the axial vorticity structures present in proximity to the model free-end.

From [7], it may also be seen that in the $2D$ case the reattachment point on the leeward face moves upstream with increasing θ, up to $\theta = 67.5^\circ$, at which a completely attached flow over the two lateral faces is present. This particular wind direction corresponds to the line bisecting the cross-section angle set against the incoming flow and a negligible cross-flow force is indeed detected in the present experimental campaign for the nearest available wind direction, i.e. $\theta = 70^\circ$. The region around this wind direction also corresponds to a plateau where the minimum drag coefficients are found.

In the $2D$ case, for $\theta > 67.5^\circ$ the stagnation point shifts to the lateral face and the largest vertical face becomes the leeward face. By increasing θ, a separation bubble is detected on the leeward surface and its reattachment point moves downstream. At $\theta = 90^\circ$ the flow is again completely separated on the leeward surface, and this wind direction corresponds to a peak of the cross-flow force coefficient.

The drag coefficient is found to increase for $\theta > 67.5^\circ$ up to $\theta \cong 120^\circ$, where a local maximum is observed. For higher values of θ, C_D decreases and reaches a local minimum at $\theta = 150^\circ$, which corresponds to a wind direction implying a reattachment of the flow on the leeward face in the $2D$ case ([7]). For the same orientation a local negative peak of the cross-flow coefficient is observed in Fig. 3(b). For $\theta > 150^\circ$ the reattachment point of the separation bubble on the leeward surface moves upstream and at $\theta = 180^\circ$ the flow is completely attached over the two lateral faces. In the range $150^\circ \leq \theta \leq 180^\circ$ the wake always detaches from the two rear vertical edges and C_D slightly increases, probably due to the widening of the wake width.

3.2 Fluctuating forces

The objective of these tests was to ascertain if the vortex shedding could produce significant fluctuating forces on the different models, and to describe their possible variation as a function of wind direction and model aspect ratio.

The first series of tests was carried out on model 60 with aspect ratio $h/w = 3.0$, by varying the wind direction in the range $0^\circ \leq \theta \leq 120^\circ$. Wavelet spectra of the cross-flow force measured at $U_\infty = 20$ m/s and different wind directions are shown in Fig. 5(a). In these spectra the high energy content at low frequencies, i.e. below St$= 0.025$, is probably connected with the wind tunnel free-stream turbulence, which is indeed characterized by an energy concentration at those low frequencies. On the other hand, the peaks in the range $0.1 \leq$ St ≤ 0.2 may confidently be associated with the alternate vortex shedding.

For this model, even if vortex shedding exists for all wind directions (as assessed from the hot-wire measurements reported in [16]), a dominant spectral component in the wavelet spectra of the cross-flow force could clearly be detected only for wind directions for which a significant streamwise extent of the afterbody is present ($0^\circ \leq \theta \leq 40^\circ$ and $80^\circ \leq \theta \leq 120^\circ$). From the wavelet spectra reported in Fig. 5(a), a decreased fluctuation energy peak is observed for $\theta = 40^\circ$ with respect to the ones detected for the remaining wind directions. This feature may be ascribed to the flow reattachment on the leeward surface occurring in the range $35^\circ \leq \theta \leq 40^\circ$.

In Fig. 5(b) the Strouhal numbers derived from the peaks in the cross-flow force spectra are compared with those obtained from the hot-wire measurements for $U_\infty = 25$ m/s, $x/w = 2.5$ and

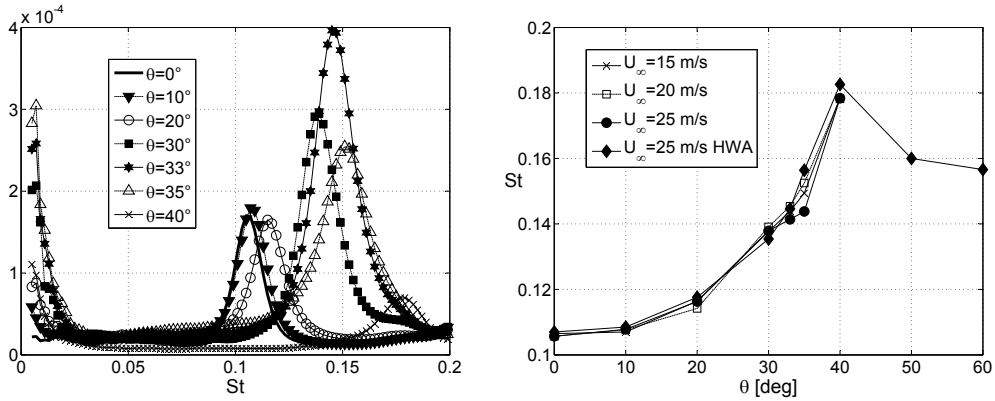

a) b)

Figure 5: Spectral characterization of cross-flow force for model 60 with $h/w = 3.0$: a) wavelet spectra measured at $U_\infty = 20$ m/s and different wind directions; b) Strouhal number connected with vortex shedding and comparison with the results obtained from the hot-wire measurements (HWA) as a function of the wind direction.

$z/h = 0.3$, described in detail in [16]. In this figure the force-related values corresponding to three different free-stream velocities, viz. 15, 20 and 25 m/s, are also shown; in effect, tests at three different velocities were carried out for this model in order to check the constancy of the Strouhal number corresponding to the spectral peaks. As can be appreciated from Fig. 5(b), the obtained values of St are practically independent from U_∞ and coincide with the hot-wire data, which is a further confirmation of the association between the fluctuating cross-flow forces and the alternate vortex shedding from the model. The remaining force measurements for all the models were then carried out for $U_\infty = 20$ m/s.

The variation with aspect ratio and wind direction of the Strouhal number derived from the peaks of the cross-flow spectra for model 60 are shown in Fig. 6(a). As can be seen, St is found to increase with decreasing aspect ratio, particularly for the two lowest values. Actually, this feature is enhanced, for all aspect ratios, approaching the wind directions at which the flow reattachment on the leeward surface occurs. This result may be ascribed to the narrowing of the wake width occurring in proximity to the model free-end, due to the flow passing over the body; thus, this three-dimensional flow characteristic seems to produce an increasing effect on the average vortex shedding frequency as the aspect ratio of the model is decreased.

As for model 90, dominating spectral components on the fluctuations of the cross-flow force were singled out for two different ranges of wind direction: $0^\circ \leq \theta \leq 60^\circ$ and $100^\circ \leq \theta \leq 150^\circ$ (Fig. 6(b)). These configurations correspond to a separated flow over the leeward surface of the model and, thus, to the presence of a significant streamwise projection of the afterbody. In the lower range of θ the values of the Strouhal numbers for model 90 are of the same order as those of model 60, which could be expected, considering that for these wind directions the cross-flow widths of both models are comparable. Conversely, for the higher range of θ the Strouhal numbers for model 90 are much higher, due to the significantly smaller cross-flow width of this model for these wind directions. Finally, the trend of the Strouhal numbers shown in Fig. 6(b) is similar to the one obtained through hot-wire measurements by [7], but with much lower values due to the flow three-dimensionality of the finite prisms. Furthermore, an increase in Strouhal number with reducing aspect ratio is also

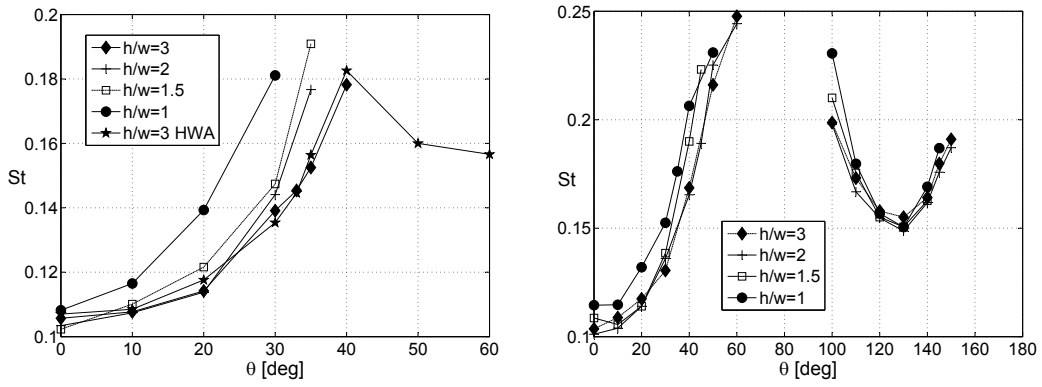

Figure 6: Strouhal numbers connected with vortex shedding, evaluated from the cross-flow force signals, for models with different cross-sections and aspect ratios: a) model 60 and hot-wire measurements (HWA); b) model 90.

found for model 90, and this feature is enhanced by approaching wind orientations for which the reattachment of the flow on the leeward surface occurs.

4 CONCLUSIONS

Triangular prisms placed vertically on a plane, having isosceles cross-section with $60°$ or $90°$ apex angles and aspect ratio, h/w, ranging from 1.0 to 3.0, were tested for wind directions, θ, varying between $0°$ and $180°$, at a prevailing Reynolds number $\mathrm{Re} = wU_\infty/\nu \cong 1.2 \cdot 10^5$.

Force measurements carried out for all models showed that the mean force coefficients decrease slightly with decreasing aspect ratio, and that for wind orientations at which the wake reattaches on the leeward vertical surface the absolute value of the mean cross-flow force may be definitely higher than the mean drag. Furthermore, the ratio between the mean drag forces acting on the prisms and those corresponding to two-dimensional bodies with the same cross-section was found to be dependent on the wind orientation, presumably in connection with differences in the free-end flow features.

The analysis of the fluctuating force signals permitted to ascertain that the vortex shedding frequency was present in the cross-flow force signals at all wind directions for which the streamwise projection of the portion of body surface immersed in the separated wake was significant. Furthermore, it was found that the vortex shedding frequency varies as a function of flow orientation in strict correlation with the variation of the width of the wake, and that it increases with decreasing aspect ratio.

References

[1] Ayoub, A. and Karamcheti, K.,"An experiment on the flow past a finite circular-cylinder at high subcritical and supercritical Reynolds-numbers," *Journal of Fluid Mechanics*, **118**, 1-26 (1982).

[2] Fox, T.A., Apelt, C.J. and West, G. S.,"The aerodynamic disturbance caused by the free-ends of a circular-cylinder immersed in a uniform-flow," *Journal of Wind Engineering and Industrial Aerodynamics*, **49**, 389-399 (1993).

[3] Kitagawa, T., Wakahara, T., Fujino, Y. and Kimura, K.,"An experimental study on vortex-induced vibration of a circular cylinder tower at a high wind speed," *Journal of Wind Engineering and Industrial Aerodynamics*, **71**, 731-744 (1997).

[4] Park, C.W. and Lee, S.J.,"Free end effects on the near wake flow structure behind a finite circular cylinder," *Journal of Wind Engineering and Industrial Aerodynamics*, **88**, 231-246 (2000).

[5] Roh, S.C. and Park, S.O.,"Vortical flow over the free end surface of a finite circular cylinder mounted on a flat plate," *Experiments in Fluids*, **34**, 63-67 (2003).

[6] Lindsey, W.F.,"Drag of cylinders of simple shapes," *NACA Report*, **619**, (1938).

[7] El-Sherbiny, S.,"Flow separation and reattachment over the side of a 90° triangular prism," *Journal of Wind Engineering and Industrial Aerodynamics*, **11**, 393-403 (1983).

[8] Luo, S.C., Yazdani, Md.G., Chew, Y.T. and Lee, T.S.,"Effects of incidence and afterbody shape on flow past bluff cylinders," *Journal of Wind Engineering and Industrial Aerodynamics*, **53**, 375-399 (1994).

[9] Alonso, G.,"Fenomenos de galope en obstaculos de section no rectangular," *Ph.D. thesis*, Universidad Politecnica de Madrid (2005).

[10] Buresti, G., Lombardi, G. and Talamelli, A.,"Low aspect-ratio triangular prisms in cross-flow: measurements of the wake fluctuating velocity field," *Journal of Wind Engineering and Industrial Aerodynamics*, **74-76**, 463-473 (1998).

[11] Buresti, G. and Lombardi, G., "Application of wavelet transform to the analysis of velocity fluctuations in the wake of triangular prisms," in *Proc.* 6^{th} *Italian Congress on Wind Engineering* (In-Vento 2000 Conference Proceedings, 2000), SGE Ed., 301-308, (2000).

[12] Iungo, G.V. and Buresti, G.,"Experimental investigation on the wake generated from a low aspect-ratio triangular prism in cross-flow," *Atti del Dipartimento di Ingegneria Aerospaziale dell'Università di Pisa*, N. ADIA 2007-4, ETS Editrice, Pisa (2007).

[13] Camarri, S., Salvetti, M.V. and Buresti, G.,"Large-eddy simulation of the flow around a triangular prism with moderate aspect-ratio," *Journal of Wind Engineering and Industrial Aerodynamics*, **94**, 309-322 (2006).

[14] Buresti, G. and Iungo, G.V., "Flow fluctuations and vorticity dynamics in the near-wake of a triangular prism in cross-flow," in *Proc. International Colloquium on Bluff Body Aerodynamics & Applications* (BBAA VI, Milano, July, 20-24, 2008), (2008).

[15] E.S.D.U.,"Mean fluid forces and moments on cylindrical structures: polygonal sections with rounded corners including elliptic shapes," *E.S.D.U.*, (Item 79026), 179-20 (1979).

[16] Iungo, G.V. and Buresti, G.,"Experimental investigation on the aerodynamic loads and wake flow features of low aspect-ratio triangular prisms at different wind directions," in press in *Journal of Fluids and Structures*, (2009).